

Effect of Heat Treatment Time on Electrochemical Performance of $\text{LiMg}_{0.04}\text{Mn}_{1.96}\text{O}_4$ cathode Materials Synthesized by a Solid-State Combustion Method

Jintao Liu^{1,2,3}, Jiabin Hao^{1,2,3}, Junming Guo^{1,2,3,*}, Changwei Su^{1,2,3,*}, Rui Wang^{1,2,3}

¹ Key Laboratory of Comprehensive Utilization of Mineral Resources in Ethnic Regions, Yunnan Minzu University, Kunming 650500, PR China

² Key Laboratory of Resource Clean Conversion in Ethnic Regions, Education Department of Yunnan, Yunnan Minzu University, Kunming 650500, PR China

³ Joint Research Centre for International Cross-border Ethnic Regions Biomass Clean Utilization in Yunnan, Yunnan Minzu University, Kunming 650500, PR China

*E-mail: guojunming@tsinghua.org.cn

Received: 15 January 2016 / Accepted: 28 February 2016 / Published: 4 June 2016

$\text{LiMg}_{0.04}\text{Mn}_{1.96}\text{O}_4$ cathode materials were successfully prepared by a solid-state combustion method at temperature of 500°C for 1h and then calcined at 600°C for different heat treatment time. The heat treatment time was investigated, and the crystal structure, morphologies of prepared samples were characterized by X-ray diffraction(XRD) and scanning electron microscopy(SEM). XRD results revealed that the crystallinity of prepared samples increased with increasing of heat treatment time. SEM results confirmed that the average particle size of prepared samples increased with the increasing of heat treatment time. The narrow particle size distribution of prepared samples consisted of particles in the range of 0.1-0.5 μm . The electrochemical performance of synthesized samples was studied by galvanostatic charge/discharge tests and cyclic voltammetry (CV). Results showed that the $\text{LiMg}_{0.04}\text{Mn}_{1.96}\text{O}_4$ material calcined at 600°C for 6h delivered better electrochemical properties with higher initial discharge specific capacity of 112.4mAh/g at room temperature and 110.8mAh/g at 55°C at 0.2C rate, and the capacity retention rates were 93.0% after 40 cycles at room temperature and 70.58% after 45 cycles at 55°C at 0.2C rate, respectively.

Keywords: Solid-State combustion method; Mg-doping; LiMnO_4 ; Heat treatment time; Lithium ion batteries

1. INTRODUCTION

It is well-known that lithium ion batteries have attracted universal interest for electric vehicles (EVs) and hybrid electric vehicles (HEVs) due to their high energy and power densities[1].

The spinel LiMnO_4 with a three-dimensional tunnel structure for the rapid migration of lithium ions has been considered to be one of the promising cathode materials to substitute for layered LiCoO_2 [2-5], which ascribed to its high operating voltage, resource abundant, low synthesis cost, low toxicity, and excellent voltage profile[6-7]. Unfortunately, the LiMn_2O_4 material presents poor cycling stability and capacity retention, especially at a higher temperature above 55°C [8]. There are three primary reasons to explain the capacity fading: the manganese dissolution caused by the corrosive reaction between LiMn_2O_4 and electrolyte into electrolyte solution; the Jahn-Teller effect out of the deep discharging to distort the crystal lattice by more Mn^{3+} and the decomposition of electrolyte solution in the higher voltage region[9-10]. To improve the cycling performance of LiMn_2O_4 as a cathode material, various methods have been proposed. The common method is bulk doping, some transition and non-transition metal elements are found to be effective to enhance the structure stability of spinel LiMn_2O_4 by partial substitution Mn with these metal species, such as Mg[11], Al[12], Ni[13], Co[14], Li[15], Cr[16], Cu[17], Zn[18], Fe[19] and Ti[20] ions. Among these elements, Mg has attracted much attention as it is eco-friendly, low-cost, resource-rich and especially lighter than other elements. In addition, the preparation method is a crucial factor that affects the electrochemical performance of spinel LiMn_2O_4 cathode material. Many approaches, such as solid-state reaction [21], sol-gel method [22], co-precipitation method[23], hydrothermal method [24], solid-state combustion synthesis[25] and so on have been developed to prepare cathode materials. The solid-state combustion synthesis has the advantages of rapid synthesis and simple process of spinel LiMn_2O_4 at a low temperature [25,26]. Xiang et al.[27] rapidly synthesized a series of $\text{LiMg}_x\text{Mn}_{2-x}\text{O}_4$ ($x \leq 0.20$) cathode material at a low temperature of 500°C for 1h by a solid-state combustion method. The results showed that the Mg-doped LiMn_2O_4 possessed better cycling stability, for the $\text{LiMg}_{0.08}\text{Mn}_{1.92}\text{O}_4$ product, its initial discharge specific capacity was 99.3mAh/g and remained 92.5mAh/g after 150^{th} cycles at 0.2C rate. Furthermore, Xiang et al.[28] also prepared $\text{LiMg}_{0.08}\text{Mn}_{1.92}\text{O}_4$ cathode materials by a solid-state combustion synthesis at different calcination temperatures. The results showed that the as prepared samples calcined at 600°C and 700°C demonstrated excellent electrochemical performance with an initial discharge specific capacity of 101.3mAh/g and 107mAh/g , and their capacity retention was 98.1% and 94.3% after 40^{th} cycles at 0.2C rate. However, the effect of further heat treatment time on the electrochemical performance of Mg-doped LiMn_2O_4 cathode material has still not been investigated by solid-state combustion method.

In this work, $\text{LiMg}_{0.04}\text{Mn}_{1.96}\text{O}_4$ cathode materials were prepared by solid-state combustion method calcined at 500°C for 1h at first, and then calcined at 600°C for different heat treatment time with manganese carbonate and lithium carbonate as raw materials, magnesium acetate as Mg^{2+} dopant and citric acid as a fuel. The effect of heat treatment Time on the crystal structure, morphology and electrochemical performance of $\text{LiMg}_{0.04}\text{Mn}_{1.96}\text{O}_4$ cathode material were investigated.

2. EXPERIMENTAL

2.1 Preparation of $\text{LiMg}_{0.04}\text{Mn}_{1.96}\text{O}_4$ cathode material

$\text{LiMg}_{0.04}\text{Mn}_{1.96}\text{O}_4$ products were prepared by a solid-state combustion synthesis. At first, lithium carbonate (AR, Sinopharm Chemical reagent Co.,Ltd.), manganese carbonate (AR, alading)

and magnesium acetate (AR, Sinopharm Chemical reagent Co.,Ltd.), were accurately weighted according to a stoichiometric ratio of Li:Mn:Mg=1:1.96:0.04 with a total mixture mass of 30g, and put into a 500mL polytetrafluoroethylene jar, respectively. A amount 5wt% of a total mixture mass of citric acid (AR,Sinopharm Chemical reagent Co.,Ltd.) was also added into the jar. After that, the mixture was ball-milled thoroughly by planetary ball mill with ethanol as a medium. Then drying the above mixture at 80°C in an oven, the precursor mixture was obtained in off-white powder. Subsequently, about 5.5g of the precursor mixture was placed in an alumina crucible and calcined in a muffle furnace at 500°C for 1h in air. And then cool the one-stage calcined $\text{LiMg}_{0.04}\text{Mn}_{1.96}\text{O}_4$ materials to ambient temperature. After grinding the samples, then the materials were recalcined in the muffle furnace at 600°C for 3h, 6h, 9h and 12h in air, respectively. The second-stage calcined materials in black powders were obtained after cooling naturally to ambient temperature.

2.2 Characterization of $\text{LiMg}_{0.04}\text{Mn}_{1.96}\text{O}_4$ materials

The characterization of the $\text{LiMg}_{0.04}\text{Mn}_{1.96}\text{O}_4$ powders was carried out by X-ray diffraction (XRD, D/max-TTRIII, Japan) with Cu $K\alpha$ radiation to identify the crystal structure and the measurement range was from 10° to 70° with 0.02° step size and scan speed was 4° min⁻¹ at an operation current of 30mA and voltage of 40kV. The particle morphology of $\text{LiMg}_{0.04}\text{Mn}_{1.96}\text{O}_4$ powders was observed by scanning electron microscopy (SEM, QUANTA-200 American FEI Company).

2.3 Electrochemical Studies of $\text{LiMg}_{0.04}\text{Mn}_{1.96}\text{O}_4$ materials

Electrochemical characterization was performed on electrodes prepared as follows. As-prepared $\text{LiMg}_{0.04}\text{Mn}_{1.96}\text{O}_4$ powder, polyvinylidene fluoride(PVDF) and acetylene black were mixed at a quantity score ratio of 80:10:10. After adding an appropriate amount of N-methyl pyrrolidinone(NMP) solvent, the mixture was mixed uniformly with a planetary ball mill. The obtained slurry was coated on the aluminum foil using a doctor-blade technique, then dried at 80°C for 4h in an oven and cut into disks with 16mm diameter. All as-prepared cathode disks were dried at 120°C in vacuum oven for overnight before cell assembling. The coin cells(CR 2025) were assembled with Li as the negative electrode and counter electrode, Celgard 2320-type membranes as the separator, 1M LiPF_6 in ethylene carbonate(EC)-1,2-dimethyl carbonate(DMC) as the electrolyte (EC and DMC volume ratio of 1:1) in a dry glove box filled with high purity argon gas. Galvanostatical charge-discharge experiments were performed by a Land electric test syetem CT2001A (Wuhan Jinnuo Electronics Co., Ltd.) between 3.20-4.35V (vs. Li/Li⁺). Cyclic voltammogram(CV) tests were carried out on ZAHNER Zennium IM6 Electrochemical Workstation (ZAHNER-elektrik GmbH & Co. KG, Kronach, Germany) from 3.60 to 4.50V (vs. Li/Li⁺) with a scan rate of 0.05mV s⁻¹. The $\text{LiMg}_{0.04}\text{Mn}_{1.96}\text{O}_4$ was used as cathode material and metallic lithium as the counter and reference anode.

3. RESULTS AND DISCUSSION

3.1 Analysis of structure

The typical XRD patterns for $\text{LiMg}_{0.04}\text{Mn}_{1.96}\text{O}_4$ samples at 500°C for 1h and then heat treatment at different time are shown in Fig.1.

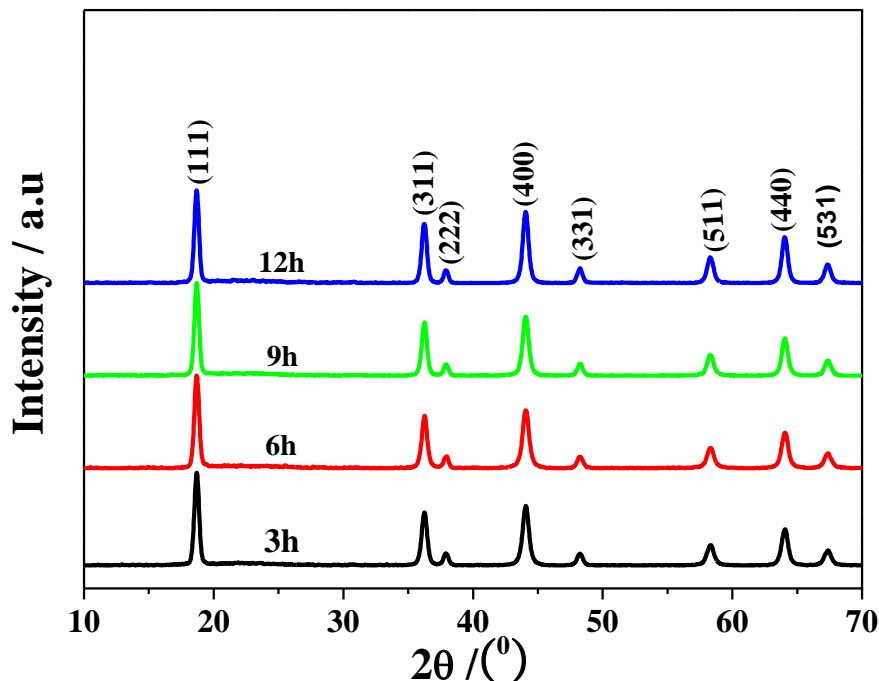


Figure 1. XRD patterns of $\text{LiMg}_{0.04}\text{Mn}_{1.96}\text{O}_4$ samples for the different heat treatment time.

It can be seen that all the samples show the well-defined XRD pattern of a cubic spinel LiMn_2O_4 phase with a space group $\text{Fd}3\text{m}$ (PDF35-0782), corresponding to eight typical crystal planes of (111), (311), (222), (400), (331), (511), (440) and (531), where lithium ions were located on the 8a sites, manganese ions resided at the 16d sites and oxygen ions occupied the 32e sites[29]. Since no impurity peaks are observed in the XRD patterns, which suggesting that the addition of Mg did not change the spinel structure of LiMn_2O_4 . The radius of Mg^{2+} ion ($r_i=0.065\text{nm}$) approaches that of Mn^{3+} ion ($r_i=0.066\text{nm}$), it can be acknowledged that Mn^{3+} ion is successfully substituted by Mg^{2+} ion. Moreover, with the increasing of heat treatment time, the diffraction peaks of $\text{LiMg}_{0.04}\text{Mn}_{1.96}\text{O}_4$ became sharper, the intensity of diffraction peaks became stronger and the full width at half-maximum (FWHM) became slightly narrower. This result implied that increasing the heat treatment time can facilitate the development of grain and enhance the crystallinity of grain. More importantly, the good crystallinity of grain implies excellent electrochemical performance.

3.2 Analysis of morphology

Fig.2 shows the SEM images of $\text{LiMg}_{0.04}\text{Mn}_{1.96}\text{O}_4$ samples at the different heat treatment time. All samples present irregular sharp particles and no significant difference with Mg substitution is observed, except for changes in particle size.

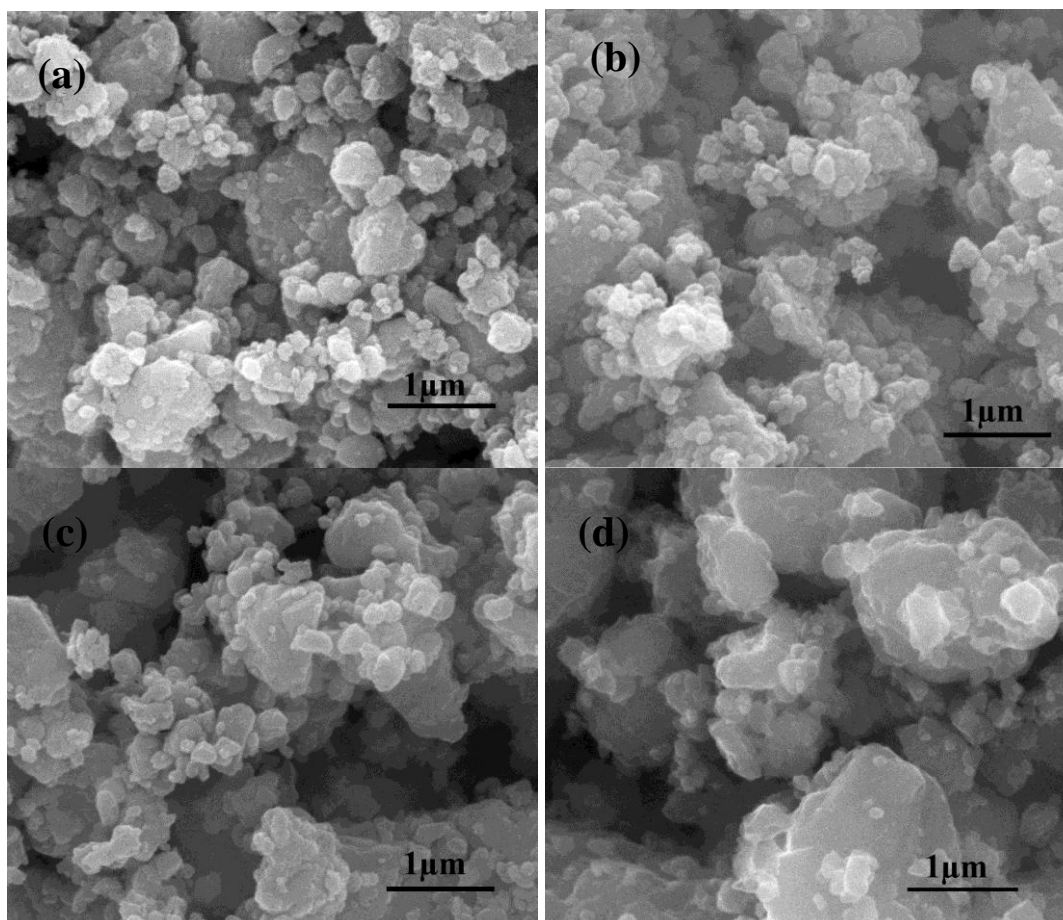


Figure 2. SEM images of $\text{LiMg}_{0.04}\text{Mn}_{1.96}\text{O}_4$ samples at the different heat treatment time for a:3h, b:6h, c:9h and d:12h.

It can be seen from Fig.2 that all the samples are made up of micron-sized secondary particles in the range of $0.8 \sim 1.5 \mu\text{m}$ formed by the primary particles aggregating together, the narrow particle size distribution is important for good electrochemical. Furthermore, when heat treatment time is 3h, the particles possess good scattered property, the outline and boundary of particles is clearly. However, with the calcination time increasing from 6h to 12h, the particles agglomerate seriously and the outline and boundary of particles become fuzzy. This situation is that as the heat treatment time increasing, the particles develop more completely and the size of particles becomes bigger. Therefore, increasing the heat treatment time is in favor of the secondary nucleation and morphology control of the primary particles to obtain the micro-sized structure and larger secondary particles. What is more, the micro-sized structure and larger secondary particles possess smaller specific area, which could decrease the

direct contact area between active materials and electrolyte, which will accordingly prevent Mn dissolving from active materials into electrolyte and achieve better cycle performance[2].

3.3 Analysis of battery performance

3.3.1 Analysis of cycling performance

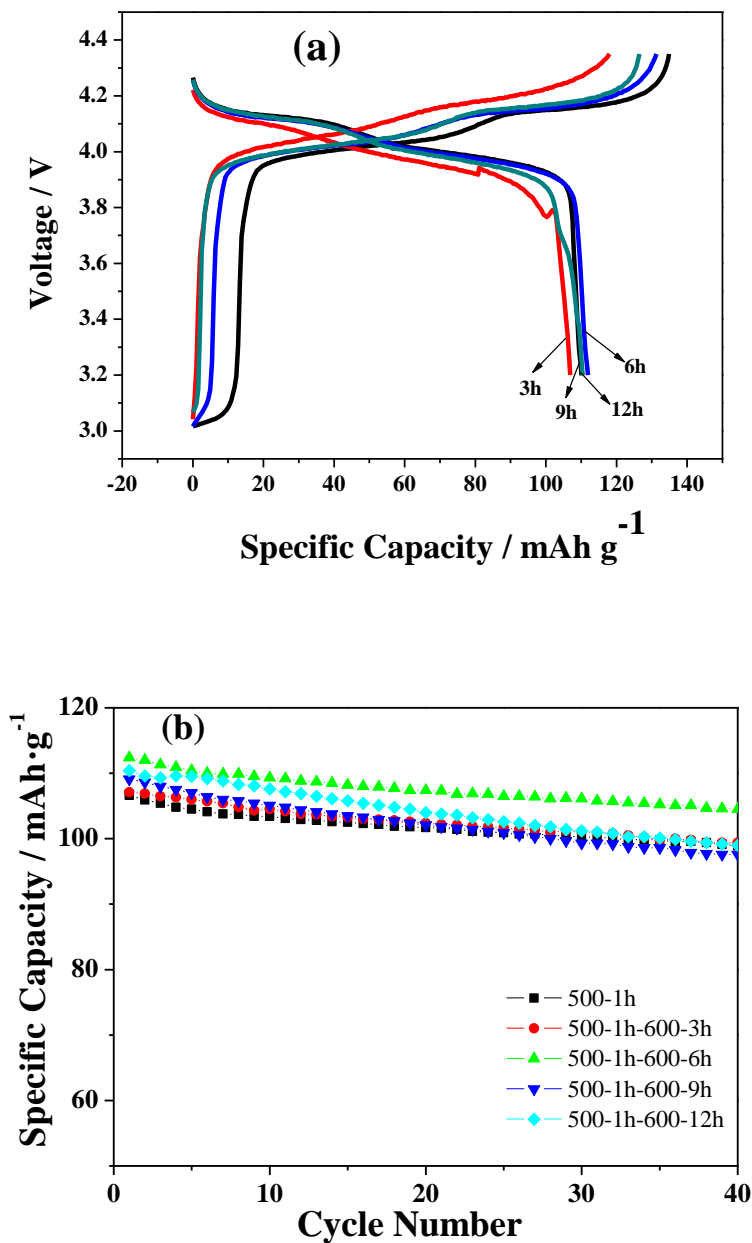


Figure 3. First galvanostatic charge-discharge curves(a), cycling performance curves (b) of $\text{LiMg}_{0.04}\text{Mn}_{1.96}\text{O}_4$ samples in the voltage range of 3.20-4.35V at 0.2C rate at room temperature.

Fig.3 displays the first galvanostatic charge-discharge profiles(a) and cycling performance curves (b) of $\text{LiMg}_{0.04}\text{Mn}_{1.96}\text{O}_4$ samples at the different heat treatment time at 0.2C rate and in the voltage range of 3.20-4.35V at room temperature.

As shown in Fig.3(a), all the charge-discharge curves exhibit two typical potential plateaus at about 4.0V and 4.1V, which suggests a obvious characteristic of a well-defined spinel LiMn_2O_4 with a second-stage mechanism for lithium extraction and insertion[30]. The initial and 40th discharge capacities and capacity retention at different heat treatment time are summarized in table 1.

Table 1. Discharge specific capacity and capacity retention rate of $\text{LiMg}_{0.04}\text{Mn}_{1.96}\text{O}_4$ samples at 0.2C rate under room temperature.

Sample	Heat treatment time /h	Discharge capacity/mAh/g		Capacity retention rate/%
		Initial	40th	
$\text{LiMg}_{0.04}\text{Mn}_{1.96}\text{O}_4$	3	107.1	99.4	92.8
	6	112.4	104.5	93.0
	9	109.1	97.6	89.4
	12	110.4	99.0	89.7

As shown in Fig.3(b) and table 1, the initial discharge specific capacity and capacity retention tend to reduce after the increase with the increase of heat treatment time. The initial discharge specific capacities for $\text{LiMg}_{0.04}\text{Mn}_{1.96}\text{O}_4$ are 107.1 mAh/g at 3h, 112.4 mAh/g at 6h, 109.1 mAh/g at 9h, 110.4 mAh/g at 12h. It delivers the discharge specific capacities of 99.4, 104.5, 97.6, and 99mAh/g after 40 cycles at a heat treatment time of 3, 6, 9, and 12h respectively. Therefore the $\text{LiMg}_{0.04}\text{Mn}_{1.96}\text{O}_4$ sample at heat treatment time 6h has best the initial specific capacity and capacity retention, which is caused by increasing the heat treatment time, the crystallinity of grain can be enhanced. The larger secondary particles have higher crystallinity of grain, however, these big particles provide longer pathways for the Li^+ diffusion and migration in charge/discharge. Therefore, the bigger particles imply inferior cycling performance.

The initial charge-discharge curves of $\text{LiMg}_{0.04}\text{Mn}_{1.96}\text{O}_4$ at different heat treatment time at 0.2C rate and between 3.20 to 4.35V at elevated temperature(55°C) are shown in Fig4.(a). All the charge-discharge curves exhibit two distinguished charge-discharge plateaus even at elevated temperature(55°C), which are ascribed to two-phase transition of $\text{MnO}_2/\text{Li}_{0.5}\text{Mn}_2\text{O}_4$ at 4.0-4.1V vs. Li/Li^+ and $\text{Li}_{0.5}\text{Mn}_2\text{O}_4/\text{LiMn}_2\text{O}_4$ at about 3.9-4.0V vs. Li/Li^+ , respectively[31].

The cycle performance of $\text{LiMg}_{0.04}\text{Mn}_{1.96}\text{O}_4$ sample at different heat treatment time at 0.2C rate at elevated temperature(55°C) are shown in Fig4.(b), and the the relevant dates are listed in table 2. It can be found that the initial discharge specific capacities for $\text{LiMg}_{0.04}\text{Mn}_{1.96}\text{O}_4$ are 112.7 mAh/g at 3h, 110.8 mAh/g at 6h, 110.1 mAh/g at 9h, 113.3 mAh/g at 12h, and the discharge specific capacities of 79.7, 78.2, 71.5, and 73.5 mAh/g after 45 cycles at a calcination time of 3, 6, 9, and 12h respectively.

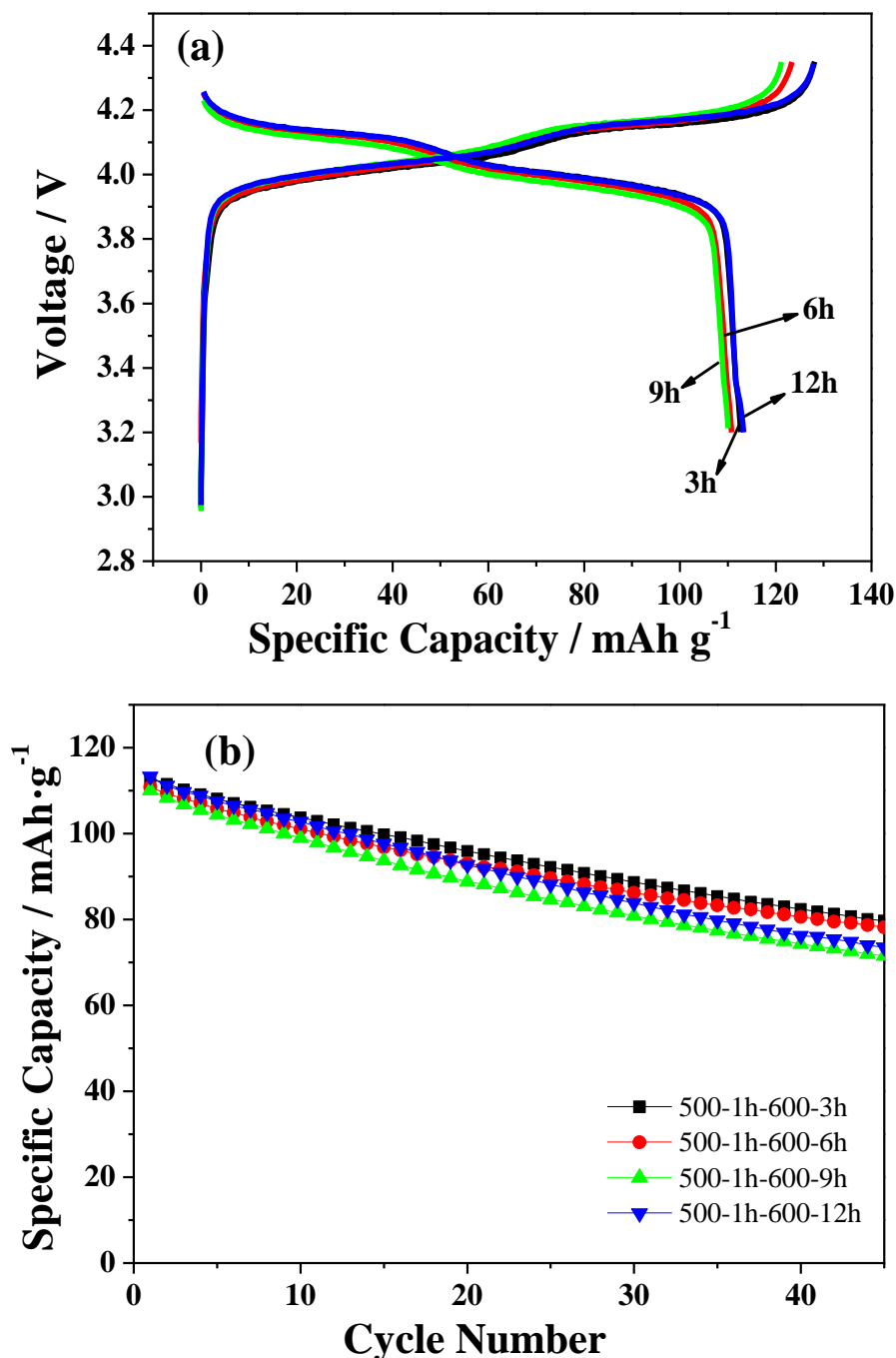


Figure 4. First galvanostatic charge-discharge curves(a), cycling performance curves (b) of $\text{LiMg}_{0.04}\text{Mn}_{1.96}\text{O}_4$ samples in the voltage range of 3.20-4.35V at 0.2C rate at elevated temperature(55°C).

It can be seen obviously that the samples at heat treatment time of 3, 6h have better cycle performance than the samples at heat treatment time of 9, 12h. The reason is that increasing the heat treatment time could enhance the crystallinity of grain, which can gain the cycling performance. However, the agglomerated morphology and bigger particles would lock Li^+ diffusion and migration, which means inferior the cycling performance. With the cycling going on, the cycling stability and discharge capacity is fading, especially at elevated temperature. The degradation of the structure during

elevated temperature cycling is due to the dissolution of Mn, which is the main reason for capacity[8-10].

Table 2. Discharge specific capacity and capacity retention rate of $\text{LiMg}_{0.04}\text{Mn}_{1.96}\text{O}_4$ samples at 0.2C rate at elevated temperature(55°C).

Heat treatment time /h	Discharge capacity/mAh/g		Capacity retention rate/%
	Initial	45th	
3	112.7	79.7	70.72
6	110.8	78.2	70.58
9	110.1	71.5	64.94
12	113.3	73.5	64.87

3.3.1 Analysis of rate performance

Fig.5 shows the reversible capacity during continuous cycling at various discharge rates(0.2C ~ 5C) at room temperature and between 3.20 to 4.35V at different heat treatment time for 3、6、9 and 12h. Compared with the discharge capacity at various discharge rates(0.2C ~ 5C), as the increasing of discharge rates from 0.2C to 5C, the discharge capacities of $\text{LiMg}_{0.04}\text{Mn}_{1.96}\text{O}_4$ sample at different heat treatment time drop gradually.

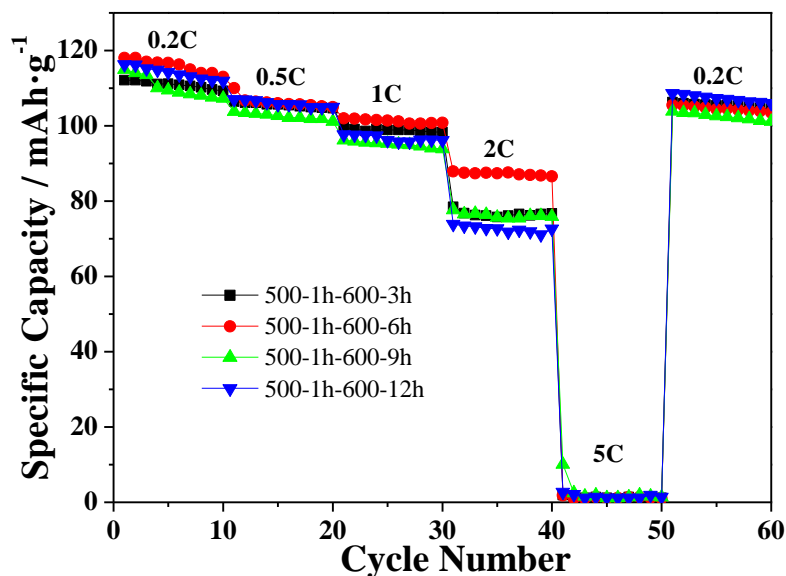


Figure 5. The rate performance curves of $\text{LiMg}_{0.04}\text{Mn}_{1.96}\text{O}_4$ samples in the voltage range of 3.20-4.35V at room temperature.

However, When increasing the current rate to 5C, the discharge capacities of prepared samples hardly discharge. The reason is that the structural stability of prepared samples invalidly enhanced at low level dopant. The result is consistent with Xiang et al.[27] test results. When decreasing current rate from 5 to 0.2C, the discharge capacities of the four cathode materials are almost restored to their initial discharge capacities at 0.2C, which indicating their good electrochemical reversibility. Compared with the four cathode materials , it can be seen that the $\text{LiMg}_{0.04}\text{Mn}_{1.96}\text{O}_4$ sample at heat treatment time 6h has better rate performance than the samples at heat treatment time 3h, 9h and 12h, which ascribed to increasing the calcination time could enhance the crystallinity of grains.

3.4 Analysis of cycling voltammetry

In addition to elucidation of the kinetics process and electrochemical cycling reversibility of synthetic materials[27,32], the four cathode materials were also measured using cycling voltammetry(CV), and the result are shown in Fig.6. There are two couples of well separated and symmetric redox peaks about at 4.09V/3.95V and 4.23V/4.10V in four voltammograms, indicating that the intercalation/ extraction of lithium ion into/from the spinel phase are reversible in the 4V region[33], corresponding to two typical potential plateaus in Fig.3(a). It can be seen from the cathodic peaks of $\text{LiMg}_{0.04}\text{Mn}_{1.96}\text{O}_4$ sample at heat treatment time 6h shift to more positive potential whereas anodic peaks shift to more negative potentials, resulting in smaller redox couple separation and the smaller potential difference(ΔE) and higher current of anodic peaks than the sample at calcination time 3h.

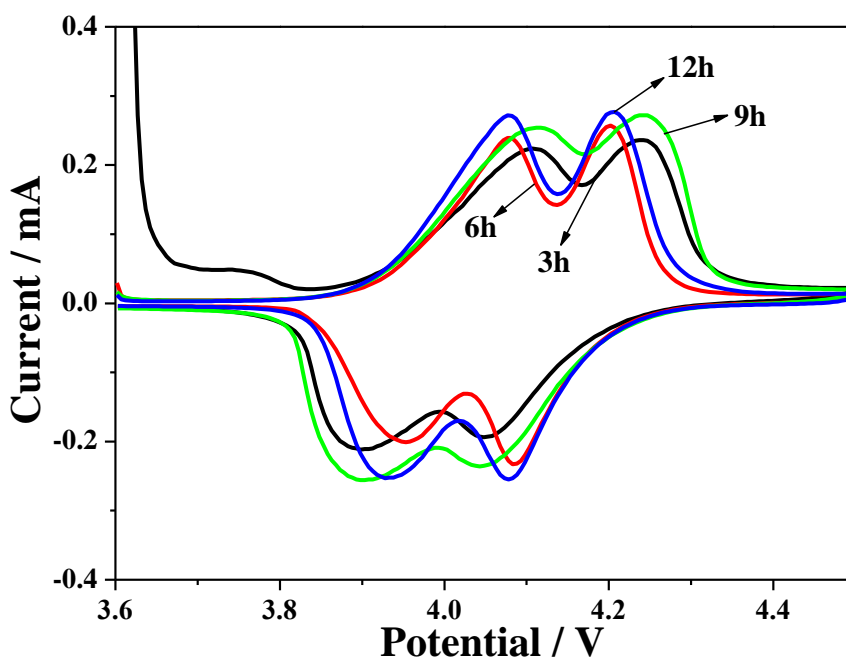


Figure 6. Cycling voltammogram curves of $\text{LiMg}_{0.04}\text{Mn}_{1.96}\text{O}_4$ samples at a scan rate of 0.05 mV/s under a voltage rang of 3.60~4.50V (vs. $\text{Li}/\text{Li}^+/\text{V}$) at room temperature.

However, compared with the CV curves at heat treatment time 9h and 12h, the cathode materials possessed larger redox couple separation and the larger potential difference (ΔE). The phenomenon may be explained that the crystallinity of the particles increased with the increasing of heat treatment time from 3h to 6h. The particles growth of the materials prepared by a too long time heat treatment were a bit larger, which restrained the Li^+ diffusion rate in the charge/discharge process. In a word, the $\text{LiMg}_{0.04}\text{Mn}_{1.96}\text{O}_4$ electrode prepared for calcination of 6h reveals the smaller electrochemical polarization, indicating the better electrochemical reversibility. The results are consistent with the cycling and rate performance results observed in Fig.3(b) and Fig.6, respectively.

4. CONCLUSIONS

Single phase $\text{LiMg}_{0.04}\text{Mn}_{1.96}\text{O}_4$ cathode materials were successfully prepared by a solid-state combustion synthesis at different heat treatment time. Its crystallinity and particle sizes increase with the increasing of heat treatment time. The particle size distribution of prepared samples consisted of particles in the range of 0.1-0.5 μm . The $\text{LiMg}_{0.04}\text{Mn}_{1.96}\text{O}_4$ sample calcined at 600 $^\circ\text{C}$ for 6h exhibited the smaller electrochemical polarization, better electrochemical reversibility, much better cycle and rate performances with higher initial discharge specific capacity of 112.4mAh/g at room temperature and 110.8mAh/g at 55 $^\circ\text{C}$ at 0.2C rate, and the capacity retention rates were 93.0% after 40 cycles at room temperature and 70.58% after 45 cycles at 55 $^\circ\text{C}$ at 0.2C rate, respectively.

ACKNOWLEDGEMENTS

This work was financially supported by the National Natural Science Foundation of China (51262031, 51462036), Program for Innovative Research Team (in Science and Technology) in University of Yunnan Province (2011UY09), Yunnan Provincial Innovation Team (2011HC008).

References

1. V. Etacheri, R. Marom, R. Elazari, G. Salitra and D. Aurbach, *Energy Environ. Sci.*, 4 (2011) 3243.
2. D. L. Guo, B. Li, Z. R. Chang, H. W. Tang, X. H. Xu, *Electrochim. Acta*, 134 (2014) 338-346.
3. M. Mohamedi, D. Takahashi, T. Itoh, I.U. Chida, *Electrochim. Acta*, 47 (2002) 3483-3489.
4. Y. Koyama, H. Arai, I. Tanaka, Y. Uchimoto and Z. Ogumi, *J. Mater. Chem. A*, 2 (2014) 11235-11245.
5. H. M. Cheng, F. M. Wang, J. P. Chu, R. Santhanam, *J. Phys. Chem. C*, 116 (2012) 7629-7637.
6. Y. L. Ding, J. Xie, G.S. Cao, T.J. Zhu, H.M. Yu, X.B. Zhao, *J. Phys. Chem. C*, 115 (2011) 9821-9825.
7. D. Tang, Y. Sun, Z. Yang, L. Gu and X. Huang, *Chem. Mater.*, 26 (2014) 3535-3543.
8. J. Molenda, M. Ziemnicki, J. Marzec, W. Zaj, M. Molenda, *J. Power Sources*, 173 (2007) 707-711.
9. T. F. Yi, Y. Xie, Y. R. Zhu, R. S. Zhu and M. F. Ye, *J. Power Sources*, 211 (2012) 59-65.
10. D. H. Jang, Y. J. Shin, S. M. Oh, *Int. J. Electrochim. Sci.*, 143 (1996) 2204.
11. G. M. Song, W.J. Li, Y. Zhou, *Materials chem. Phys.*, 87 (2004) 162.
12. L. Xiao, Y. Zhao, Y. Yang, X. Cao, X. Ai, H. Yang, *Electrochim. Acta*, 54 (2008) 545.

13. Y. J. Wei, L.Y. Yan, C.Z. Wang, X. G. Xu, F. Wu, G. Chen, *J. Phys. Chem. B*, 108 (2004) 18547-18551.
14. S. L. Zhao, H. Y. Chen, J. B. Wen, D. X. Li, *J. Alloys. Compd.*, 474 (2009) 473-476.
15. R. J. Gummow, A. Dekock, M. M. Thackeray, *Solid State Ionics*, 69 (1994) 59-67.
16. Z. D. Peng, Q. L. Jiang, K. Du, W. G. Wang, G. R. Hu, Y. X. Liu, *J. Alloys. Compd.*, 493 (2010) 640-644.
17. A. Sulochana, R. Thirunakaran, A. Sivashanmugam, S. Gopukumar, *J. Electrochem. Soc.* 155 (2008) A206-A210.
18. Arumugam D, Kalaiganan GP, Vediappan K, Lee CW, *Electrochim. Acta*, 55 (2010) 8439-8444.
19. H. Shigemura, H. Sakaebe, H. Kageyama, H. Kobayashi, A. R. West, R. Kanno, M. Tabuchi, *J. Electrochem. Soc.*, 148 (2001) A730-A736.
20. L. L. Xiong, Y. L. Xu, C. Zhang, Z. W. Zhang, J. B. Li, *J. Solid State Electrochem.*, 15 (2011) 1263-1269.
21. W. C. Wen, B. W. Ju, X. Y. Wang, C. Wu, H. B. Shu, X. K. Yang, *Electrochim. Acta*, 147 (2014) 271-278.
22. H. Y. Zhao, X. Q. Liu, C. Cheng, Z. Zhang, Y. Wu, B. Chen, W. Q. Xiong, *J. Solid State Electrochem.*, 19 (2015) 1015-1026.
23. M. H. Zhang, Y. Z. Liu, Y. G. Xia, B. Qiu, J. Wang, Z. P. Liu, *J. Alloys. Compd.*, 598 (2014) 73-78.
24. C. H. Jiang, S. X. Dou, H. K. Liu, M. Ichihara, H. S. Zhou, *J. Power Sources*, 172 (2007) 410-415.
25. X. Y. Zhou, M.M. Chen, M.W. Xiang, H.L. Bai, J.M. Guo. *Ceram. Int.*, 39 (2013) 4783-4789.
26. X. Y. Zhou, M. M. Chen, H. L. Bai, C. W. Su, L. L. Feng, J. M. Guo, *Vacuum* 99 (2014) 49-55.
27. M. W. Xiang, C. W. Su, L. L. Feng, M. L. Yuan, J. M. Guo, *Electrochim. Acta*, 125 (2014) 524-529. X. Y.
28. M. W. Xiang, L. Q. Ye, C. C. Peng, L. Zhong, H. L. Bai, C. W. Su, J. M. Guo, *Ceram. Int.*, 40 (2014) 10839-10845.
29. Y. Wang, Q. Peng, G. Yang, Z. Yang, L. C. Zhang, H. Long, *Electrochim. Acta*, 136 (2014) 450-456.
30. D. Arumugam, G. Paruthimal Kalaiganan, *J. Electroanal. Chem.*, 648 (2010) 54-59.
31. X. Yi, X. Y. Wang, B. W. Ju, Q. L. Wei, X. K. Yang, G. S. Zhou, *J. Alloys. Compd.*, 604 (2014) 50-56.
32. B. S. Qin, Z. H. Liu, G. L. Ding, Y. L. Duan, C. J. Zhang, G. L. Cui, *Electrochim. Acta*, 141 (2014) 167-172.
33. H. L. Zhang, L. Zhang, S. W. Yang, *Int. J. Electrochem. Sci.*, 9 (2014) 8182-8188.